Front. Mech. Eng. 2020, 15(3): 406–416
https://doi.org/10.1007/s11465-019-0578-2

RESEARCH ARTICLE

Yongliang YUAN, Liye LV, Shuo WANG, Xueguan SONG

Multidisciplinary co-design optimization of structural and control parameters for bucket wheel reclaimer

Abstract Bucket wheel reclaimer (BWR) is an extremely complex engineering machine that involves multiple disciplines, such as structure, dynamics, and electromechanics. The conventional design strategy, namely, sequential strategy, is structural design followed by control optimization. However, the global optimal solution is difficult to achieve because of the discoordination of structural and control parameters. The co-design strategy is explored to address the aforementioned problem by combining the structural and control system design based on simultaneous dynamic optimization approach. The radial basis function model is applied for the planning of the rotation speed considering the relationships of subsystems to minimize the energy consumption per volume. Co-design strategy is implemented to resolve the optimization problem, and numerical results are compared with those of sequential strategy. The dynamic response of the BWR is also analyzed with different optimization strategies to evaluate the advantages of the strategies. Results indicate that co-design strategy not only can reduce the energy consumption of the BWR but also can achieve a smaller vibration amplitude than the sequential strategy.

Keywords bucket wheel reclaimer, co-design, energy-minimum optimization, sequential strategy

1 Introduction

Bucket wheel reclaimer (BWR) is a large complex engineering machine that is widely used in open pit mines because of its many excellent advantages, such as high efficiency, low labor strength, and easy operation. However, the working condition of the BWR has several uncertain factors, such as falling ore and surface irregularity. A large amount of resources is also consumed by the operation of the BWR because of the sub-optimal size of the BWR structure, such as too heavy weight and high power consumption. Therefore, improving the performance and decreasing the energy consumption of BWR are still challenging tasks.

Many researchers have focused on improving the performance of the BWR and preventing accidents. For example, the integrity assessment of the bucket wheel tie-rod is calculated in Ref. [1]. The causes of failure through onsite inspection and metallographic analysis are achieved in Ref. [2]. The cause of crack occurrence and stress strain state is obtained using the finite element method [3]. Although the performance of the BWR can be improved by considering the cutting force, stress strain state, and structural improvement, the optimal control problem is still an important factor that must be considered. To this end, a hybrid controller to control the motion for enhancing the performance of the BWR is proposed by Lu [4,5]. Reclaiming method of the BWR adopts the pilgrim step reclaiming approach. Unscented Kalman filter algorithm is proposed by Zhao et al. [6] to fuse differential global positioning system and encoder data for improving the performance of the BWR.

The works above indicate that the structural improvement and optimal control on the BWR are conducted separately. For this reason, the optimization problem of the BWR usually adopts the following sequential strategy, that is, the control optimization is performed after the structural optimization is completed. This optimization strategy ignores the coupling relationship between structural and control parameters and can only achieve a sub-optimal solution. This study uses the co-design strategy to solve the optimization problem for addressing this challenge by considering structural and control parameters. A novel collaborative optimization (CO) method is used to optimize the train stop planning and scheduling on the tactic level [7]. The belt drive optimization problem is

Received August 20, 2019; accepted November 18, 2019

Yongliang YUAN, Liye LV, Shuo WANG, Xueguan SONG (✉)
School of Mechanical Engineering, Dalian University of Technology, Dalian 116024, China
E-mail: sxg@dlut.edu.cn

solved with the CO strategy to obtain the optimal parameters for each sub-discipline [8]. A multi-physical field CO method based on Genetic Algorithm is proposed by Li et al. [9] to improve the utilization of materials and reduce cost. The CO approach is applied to minimize the total pumping power consumption for a typical heat transfer system in Ref. [10].

However, BWR is a complicated system that usually includes many sub-disciplines, such as dynamics, electro-mechanics, and fluid dynamics. For this reason, this work considers the coupling relationship of the sub-disciplines. The co-design strategy is conducted to obtain the optimal solution and balance the relationship among the sub-disciplines. Co-design has been successfully applied in many fields. For example, co-design is applied to optimize the parameters of the tunnel boring machine (TBM) for improving the performance of TBM [11,12]. A reliability-based multidisciplinary design optimization method is used to optimize an aerial camera and a car pad [13]. Bidoki et al. [14] proposed a novel optimization design framework based on co-design to optimize the autonomous underwater vehicle. The results show that the co-design strategy can achieve the global optimal solution. Although the performance of the BWR has been intensively studied, researchers have mainly focused on optimizing the structural or control parameters and ignored the coupling relationship of structure, control, and other disciplines of the BWR. This study utilizes the co-design strategy to improve the performance of the BWR for considering the coupling relationship among these disciplines and obtaining the comprehensive performance of the BWR. The aim is to obtain the optimal structural and control parameters.

The remainder of this work is organized as follows. Section 2 introduces the composition of the BWR. Section 3 discusses the configuration of the BWR subsystems. Section 4 establishes the mathematical model, and Section 5 performs numerical simulation. Section 6 summarizes the concluding remarks and future work.

2 Composition of the BWR

2.1 System analysis of the BWR

BWR integrates multiple sub-disciplines, and its performance depends on the synergy of the components. Figure 1 shows that a BWR consists of subsystems, including the structural, control, and vibration systems. Notably, each subsystem can be categorized into various separate disciplines. For example, the structural system consists of structure and dynamics. Some "soft subsystems," such as energy consumption, also exist. As mentioned above, the performance of the BWR is directly determined by the coordination of these disciplines.

2.2 Excavation strategies

Constant volume excavation is needed in the excavation process to ensure the minimum impact force on the BWR. The excavation operation can be categorized into two strategies according to the excavation technology, including hierarchical (Fig. 2(a)) and fixed-point (Fig. 2(b)) operations.

Figure 2(a) shows that the BWR performs with a layered manner and obtains the feed rate by rotary motion. The

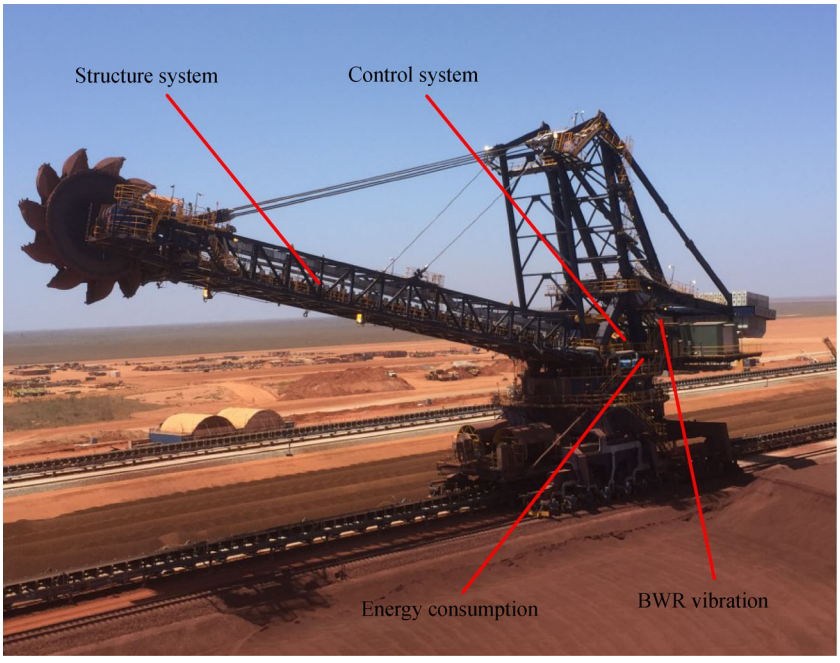

Fig. 1 Whole structure of the bucket wheel reclaimer.

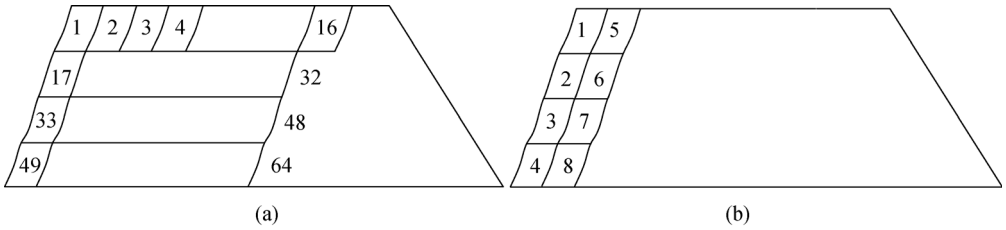

Fig. 2 Excavation technology of the bucket wheel reclaimer: (a) Hierarchical and (b) fixed-point operations.

bucket wheel system will move downward with the action of the pitching system when the current height is excavated. The excavation process of the fixed-point operations is illustrated in Fig. 2(b), which is distinct from the hierarchical operation. Notably, the BWR system is applied to excavate the ore pile from top to bottom. The bucket wheel system will rotate with the action of the rotating system when the current region is excavated. However, the latter strategy is worse than the former. The reason is that the latter is prone to collapse. Thus, the former strategy is adopted in this study to excavate the ore pile efficiently and safely.

3 Configuration of the BWR subsystems

3.1 Control system

Figure 3(a) shows that the BWR can be simplified into a manipulator with four degrees of freedom, where d_1 is the translation distance along joint "j_1", θ_2 is the slewing angle rotating about joint "j_2", θ_3 is the luffing angle rotating about joint "j_3", and θ_b is bucket wheel rotation angle rotating about "j_4". The red curve in Fig. 3(b) is the excavation trajectory, which is dictated by one hydraulic device and two motors. Although the excavator trajectory of the BWR can be obtained on the basis of the Danevit–Hartennberg (D–H) method, it only refers to the relationship among structural parameters. The control parameters should be considered to obtain the excavation optimal trajectory with the minimum energy consumption.

Various trajectory optimization methods have been proposed in the past decade. For example, Garg et al. [15] proposed the global collocation of Legendre–Gauss–Radau method to optimize the trajectory. A novel trajectory optimization method, namely, Monte Carlo motion planning, is applied to solve the motion planning under uncertainty [16]. The point-to-point trajectory planning method is used to realize the energy minimum for the large cable shovel [17]. Tian and Collins [18] proposed a polynomial based on Hermite cubic interpolation method to realize the obstacle avoidance movement for the robot manipulator. Although trajectory planning has been intensively studied, the methods sometimes exhibit difficulty in obtaining optimal solutions when solving high-dimensional problems. Therefore, the trajectory planning method is still a challenging and critical research subject for many researchers. The radial basis function (RBF), which is proposed by Franke [19], is used to perform trajectory planning of the BWR in this work to address the aforementioned issue. The RBF is defined as the selection of a radial function for the given multivariate scattered data, which has been applied in previous papers [19,20]. An RBF model is an approximation of a real-valued F, which can be expressed as

$$S(x) = \sum_{i=1}^{N} a_i \Phi(\|x - x_i\|),\ x \in \boldsymbol{R}^d, \tag{1}$$

where a_i is a basis weight function, $\|(x-x_i)\|$ denotes the Euclidean distance between x and x_i, Φ is a basis function, d denotes the number of dimensions, $\boldsymbol{R}$ denotes the real number field, and $x_i\ (i = 1, 2, ..., N)$ are the centers of the RBF approximation.

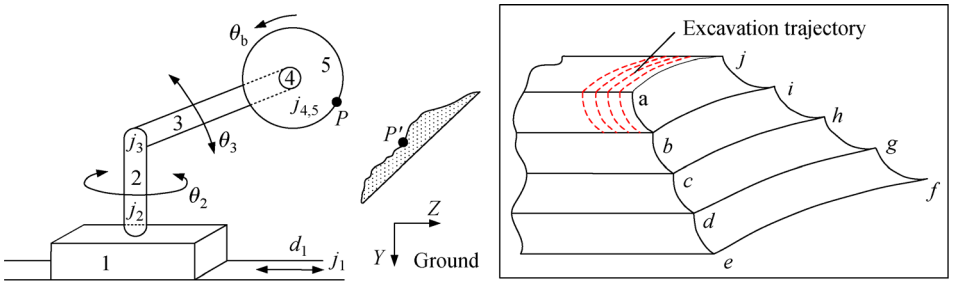

Fig. 3 (a) Schematic of bucket wheel reclaimer; (b) excavation trajectory.

The speed of the motor can be achieved indirectly by adjusting the position and number of the interpolation points. Several typical basis functions have been given by Wu and Schaback [21], such as multi-quadrics, inverse multi-quadrics, and Gaussian, as shown in Table 1. In this work, the multi-quadrics is selected to optimize the speed of the motor.

Table 1 Choices of Φ for the interpolation matrix

Basis function	$\Phi(x)$
Multi-quadrics	$(x^2+\delta^2)^{1/2},\ \delta\geqslant 0,$
Inverse multi-quadrics	$(x^2+\delta^2)^{-1/2},\ \delta\geqslant 0$
Gaussian	$e^{-x^2/\delta^2},\ \delta\geqslant 0$

A typical speed curve of the motor can be achieved by RBF, as shown in Fig. 4. The speed of the motor can be described as follows:

$$v_c = f(\boldsymbol{x}_c),\ \boldsymbol{x}_c = [v_1, v_2, ..., v_n], \tag{2}$$

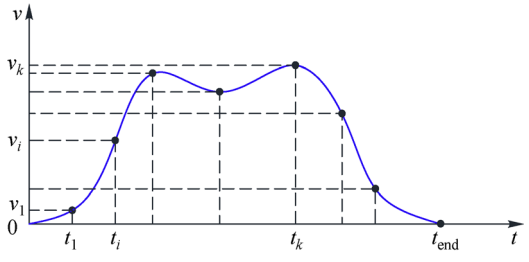

Fig. 4 Typical speed curve of the motor.

where v_c denotes the speed curve of the motor, v_i denotes the speed value of the motor in the ith position, n is the number of interpolation points, $\boldsymbol{x}_c$ is the column vector of the discrete speed set, and $f(\boldsymbol{x}_c)$ is the fitting speed curve.

The constant volume excavation strategy is usually adopted in real world to reduce the impact of vibration on the BWR. In traditional theoretical research, the ore pile is taken as a rectangle while the effect of the angle of repose is ignored [22]. However, the lateral section of the ore pile is of typical trapezoid shape due to the angle of repose. This study uses the RBF to obtain the speed of the rotating system for addressing the aforementioned challenge by considering the effect of the angle of repose and constant volume constraint.

3.2 Structural system

In conventional design, the energy-minimum optimization focuses on the optimal control parameters. This optimization is performed on the basis of fixed structural parameters. However, traditional/sequential design processes can only obtain sub-optimal results because the methods disregard the coupling between structural and control systems. Thus, this study aims to achieve the optimal solutions with the co-design for the BWR. The energy consumption of the BWR mainly comes from the movement of the rotating system. In this study, the moment of inertia is an important affecting factor of energy consumption. Therefore, we can select the parameters that affect the moment of inertia to serve as the design variables. Figure 5 illustrates the configuration of the BWR.

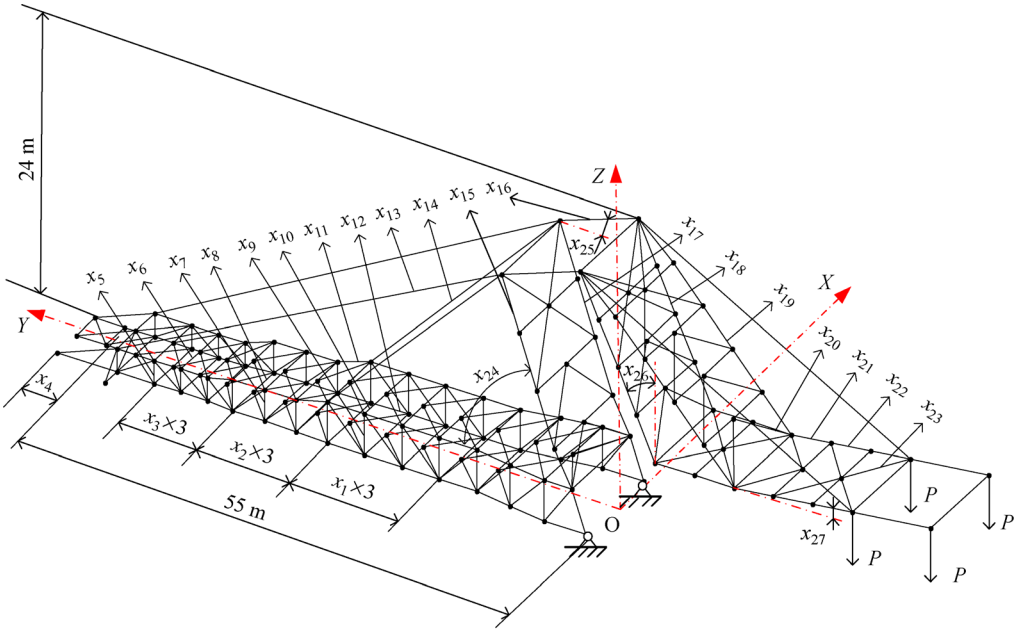

Fig. 5 Configuration of the bucket wheel reclaimer.

3.3 BWR vibration

Vibration is an inevitable phenomenon that occurs in the BWR due to the intense changes in the load. The frequent changes in the load are due to three reasons. First, the direction of rotation of the slewing mechanism changes considerably. Second, frequent acceleration and deceleration occur in the BWR. Finally, ore pile is composed of non-uniform granularities and fluctuant terrains. These vibration factors may cause the failure of the BWR and can thus result in an accident. Therefore, the influence of vibration should be considered when investigating structural and control CO based on co-design strategy. The vibration of the BWR can be expressed as

$$\boldsymbol{M}\ddot{\delta} + \boldsymbol{C}\dot{\delta} + \boldsymbol{K}\delta = f, \tag{3}$$

where $\boldsymbol{M}$, $\boldsymbol{C}$, and $\boldsymbol{K}$ denote the mass, damping, and stiffness matrixes, respectively, δ, $\dot{\delta}$, and $\ddot{\delta}$ denote the displacement, velocity, and acceleration, respectively, and f is the applied force. The damping matrix of the system is usually difficult to determine in practical engineering. The commonly used method to accurately predict the vibration performance of the system is to approximate the damping value using the energy consumed by the system, which is often obtained from actual measurements. Therefore, the damping matrix is used given the overall damping matrix of the system rather than the element damping matrix. The damping matrix is given in the form of proportional damping or Rayleigh damping due to the complexity of the BWR, and its expression can be given as follows:

$$\boldsymbol{C} = \alpha\boldsymbol{M} + \beta\boldsymbol{K}, \tag{4}$$

where α and β are constants. Proportional damping has many advantages, such as the stiffness and mass matrixes are in positive correlation. A diagonal matrix can be obtained on the basis of this advantage.

$$\boldsymbol{\varphi}_j^{\mathrm{T}}\boldsymbol{C}\boldsymbol{\varphi}_i = \begin{cases} c_i & i = j, \\ 0 & i \neq j, \end{cases} \tag{5}$$

where $\boldsymbol{\varphi}_j^{\mathrm{T}}\boldsymbol{C}\boldsymbol{\varphi}_i$ denotes the diagonal matrix. Equation (3) can be equivalently transformed with the modal matrix as follows:

$$\ddot{\eta}_i + 2\xi_i\omega_i\dot{\eta}_i + \omega_i^2\eta_i = f_i,\ i = 1, 2, ..., n, \tag{6}$$

where ξ_i denotes the damping ratio and η_i is the amplitude of vibration at time i. The solution of Eq. (6) can be expressed as follows:

$$\begin{aligned} \eta_i(t) = {} & \eta_i(t_0)\mathrm{e}^{-\xi_i\omega_i t}\cos\omega_{\mathrm{d}}t \\ & + \frac{\dot{\eta_i}(t_0) + \xi_i\omega_i\eta_i(t_0)}{\omega_{\mathrm{d}}}\mathrm{e}^{-\xi_i\omega_i t}\sin\omega_{\mathrm{d}}t \\ & + \frac{1}{\omega_{\mathrm{d}}}\int_{t_0}^{t}\mathrm{e}^{-\xi_i\omega_i(t-\tau)}\sin\omega_{\mathrm{d}}(t-\tau)f_i(\tau)\mathrm{d}\tau, \end{aligned} \tag{7}$$

where $\omega_{\mathrm{d}} = \omega_i\sqrt{1-\xi^2}$ denotes the natural frequency with damping, ω_i represents the natural frequency without damping, t denotes the simulation time, and τ is the time increment.

BWR is a repeated rotating motion machine. Thus, the impact force can be simplified into a simple harmonic excitation. The solution can be given by

$$\begin{aligned} \eta_i(t) = {} & \eta_i(0)\mathrm{e}^{-\xi_i\omega_i t}\cos(\omega_{\mathrm{d}}t) \\ & + \frac{\dot{\eta_i}(0) + \xi_i\omega_i\eta_i(0)}{\omega_{\mathrm{d}}}\mathrm{e}^{-\xi_i\omega_i t}\sin(\omega_{\mathrm{d}}t) \\ & - X\mathrm{e}^{-\xi_i\omega_i t}\left(\frac{\xi_i\omega_i\cos\psi + \omega\sin\psi}{\omega_{\mathrm{d}}}\sin(\omega_{\mathrm{d}}t) + \cos\psi\cos(\omega_{\mathrm{d}}t)\right) \\ & + X\cos(\omega t - \psi), \end{aligned} \tag{8}$$

where γ denotes the ratio of the frequency of the payload to the natural frequency without damping.

$$X = \frac{f_{0i}}{\omega_i^2}\frac{1}{\sqrt{(1-\gamma^2)^2 + (2\xi_i\gamma)^2}}, \tag{9}$$

$$\psi = \arctan\frac{2\xi_i\gamma}{1-\gamma^2}. \tag{10}$$

3.4 Energy consumption

As mentioned above, the energy consumption of the BWR is mainly determined by the rotating system, which consumes more energy than other systems. The co-design strategy is explored to overcome this issue by combining the structural and control parameters. With the gradually diminishing crude oil resource, the optimization of energy consumption has been become a major topic. Constant volume constraint and energy consumption are considered together to establish the evaluation index presented in this section. The energy consumption index per volume (E_{p}, kW/m^3) is adopted to evaluate the index of the BWR conveniently and can be calculated as follows:

$$E_{\mathrm{p}} = \frac{E_{\mathrm{t}}}{Vol}, \tag{11}$$

where E_{t} denotes the total energy consumption (unit: kW), and Vol denotes the total volume (unit: m^3). The energy consumed of the motor is another notable constraint, and it can be calculated using the integral:

$$E_{\mathrm{m}} = \int_{t_0}^{t_{\mathrm{f}}} F(t)\cdot v(t)\mathrm{d}t, \tag{12}$$

where $F(t)$ is the momentary force output from the motor (unit: N), and $v(t)$ is the speed of the motor (unit: rad/s). Notably, the cutting resistance and gravity are the main influencing factors of the performance of the motor. The

cutting resistance F can be decomposed into three parts, namely, the tangential force F_1, normal force F_2, and lateral force F_3:

$$\begin{cases} F_1 = P_1\left(\Delta\cos\psi - \theta\sin\psi - \cot(\alpha_k - \Delta + \rho)\cos\psi\right) + P_2\cos\psi, \\ F_2 = P_1[1 + \Delta\cot(\alpha_k - \Delta + \rho)] + P_2(\tan\rho + \delta_k), \\ F_3 = 0.3F_1, \end{cases} \tag{13}$$

where P_1 is the force on the front edge of the tooth (unit: N), P_2 is the force on the back edge of the tooth (unit: N), Δ denotes the correction value of the front clearance angle and the back angle (unit: (°)), ψ is the projection of the main cutting edge and the rotor rotation axis (unit: (°)), θ denotes the inclination angle of the bucket wheel (unit: (°)), α_k is the front angle (unit: (°)), ρ is the friction angle (unit: (°)), and δ_k denotes the angle of deviation of the dulling plane (unit: (°)).

The resistances can be obtained and described in detail by Chudnovskii [23]. Figure 6 presents the resistance analysis of the BWR.

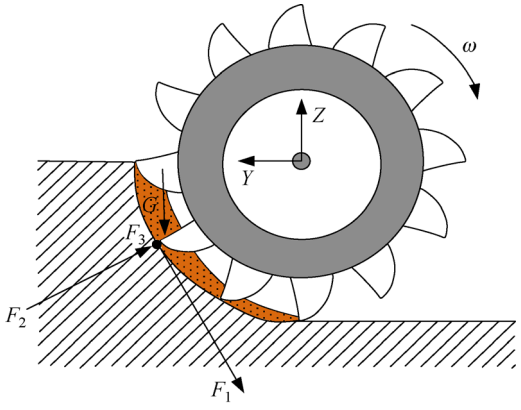

Fig. 6 Resistance analysis of the bucket wheel reclaimer.

The performance of the motor is directly reflected in the speed and torque. The characteristic of the motor must be considered in the energy consumption optimization problem. The red imaginary and blue solid lines in Fig. 7

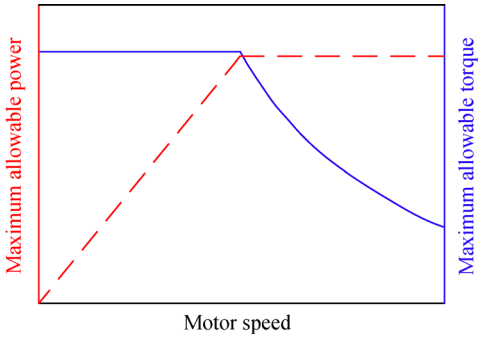

Fig. 7 Characteristic curve of the motor.

are the maximum allowable power ($P_{\max}$) and torque ($T_{\max}$), respectively. The actual power (P_a) and torque (T_a) should be less than the motor rate to ensure the safety of the motor. According to the above-mentioned analysis, the following equation for power and torque can be obtained:

$$\begin{cases} P_a - P_{\max} \leqslant 0, \\ T_a - T_{\max} \leqslant 0. \end{cases} \tag{14}$$

4 Model establishment

Co-design strategy is marked by obtaining an optimal system. The energy consumption of the BWR is mainly in the rotating system, which includes structural and control parameters. Therefore, the product of the moment of inertia and angular velocity is preserved as the objective function. As mentioned in Section 3.1, the RBF is adopted to match the motor speed curve. Thus, inserting values can be selected to serve as the control parameters, which are determined by optimizing the RBF model.

The moment of inertia is affected by certain structural parameters, such as the length, width, height, and cross-sectional area of I-beam, as shown in Fig. 5. With regard to the structural parameters, the angles are also preserved as the design variables. In this study, the period time for the BWR is constant. Following the above-mentioned analysis, the structural parameters $\boldsymbol{x}_s$ and control parameters $\boldsymbol{x}_c$ can be expressed as follows:

$$\boldsymbol{x} = [\boldsymbol{x}_c, \boldsymbol{x}_s] = [[v_1, v_2, \ldots, v_n], [x_1, x_2, \ldots, x_{27}]]. \tag{15}$$

This work compares the effects of different numbers of interpolation points to obtain the global optimal solution. The ranges of interpolation points are defined from zero to the maximum speed of the motor. The model of the BWR can be given by

$$\begin{aligned} &\text{find} \quad \boldsymbol{x} = [\boldsymbol{x}_c, \boldsymbol{x}_s], \\ &\min \quad f_{\text{obj}} = \frac{1}{Vol}\cdot\frac{1}{2}\cdot J(\boldsymbol{x}_s)\cdot\omega(\boldsymbol{x}_c)^2, \\ &\text{s.t.} \quad g_j \leqslant 0 \quad (j = 1, 2, 3, 4), \end{aligned} \tag{16}$$

where Vol is the excavation volume of the ore pile, ω denotes the rotational speed of the BWR's boom, and J is the moment of inertia of the BWR. As mentioned in Section 3, the constraints of the BWR consist of four sub-disciplines, which have been explained in detail. In the control system, the maximum rotor speed should be less than 0.085 rad/s. In this study, the motor efficiency is selected as 0.95. Structural parameters should not only meet the requirements of space structure but also satisfy the relationship between the BWR and the ore pile. In this study, the boundary of these parameters is set to 0.6 to 1.5 times the initial values. Notably, the constraints of the

structural parameters mainly include the length, width, height, and cross-sectional area of the beam and angles of the BWR. In addition, the maximum stress of the beam should be less than the yield strength of the steel. The motor constraints, including the actual power and torque, should be lower than the maximum allowable power and torque to minimize energy consumption. From the analysis above, the constraints of BWR can be given by

$$g = \begin{bmatrix} g_1 \\ g_2 \\ g_3 \\ g_4 \end{bmatrix} \leqslant 0, \tag{17}$$

where

$$g_1: \begin{cases} 0-\omega, \\ \omega-0.085, \\ 0-V_{\mathrm{p}}, \\ V_{\mathrm{p}}-3, \end{cases}$$

$$g_2: \begin{cases} x_{\min}-x_i, \\ x_i-x_{\max}, \\ 65^\circ-\alpha_1, \\ \alpha_1-75^\circ, \\ 6^\circ-\alpha_2, \\ \alpha_2-12^\circ, \\ 15^\circ-\alpha_3, \\ \alpha_3-21^\circ, \\ 4^\circ-\alpha_4, \\ \alpha_4-8^\circ, \\ \sigma_{\min}-\sigma_i, \\ \sigma_i-\sigma_{\max}, \end{cases} i=(1,2,...,23)$$

$$g_3: \omega_{\min} \leqslant \omega_i \leqslant \omega_{\max},\ g_4: \begin{cases} 0-P_{\mathrm{a}}, \\ P_{\mathrm{a}}-P_{\max}, \\ 0-T_{\mathrm{a}}, \\ T_{\mathrm{a}}-T_{\max}. \end{cases}$$

According to the "no free lunch" theorem [24], no single optimization algorithm can efficiently solve all problems. For this reason, many studies have focused on improving the accuracy and efficiency of the algorithms by using the new optimization strategies. In this work, we select the Coulomb force search strategy-based dragonfly algorithm (CFSSDA) to optimize the BWR. The performance of CFSSDA has been verified in Ref. [25].

5 Numerical simulation

5.1 Determination of the number of the interpolation points of RBF

In theory, the speed curve of the motor will gradually become close to the optimal solution as the number of interpolation points increases and will finally be infinitely close to the global optimal solution. However, computing cost also increases with the increase in the number of interpolation points. For this reason, the number of interpolation points should be confirmed in this section. According to the BWR performance and the motor characteristics, the number of interpolation points should not be less than five points. The main reasons for this condition are the influence of the constant volume constraint and the acceleration and deceleration times. The constraints and loads are set to be the same and the material surface angle is set to 38° to ensure a fair comparison among the different numbers of interpolation points. In this section, the optimal control parameters are optimized on the basis of fixed structural parameters. The number of interpolation points is set to 6, 8, 10, and 12. The simulation is performed 30 times independently to minimize the statistical error. Table 2 presents the influence of different interpolation points on energy consumption.

Figure 8 shows that the optimization result decreases first and then increases as the number of points increases. Specifically, the result of eight points achieves the first ranking, followed by six, ten, and twelve points. Table 2 shows that the standard deviation decreases first and then increases, which is similar to the optimization results. Notably, eight interpolation points have strong robustness. In comparison with the results of the different numbers of interpolation points, the strategy of eight interpolation points is significantly better than the other strategies.

Table 2 The influence of the different interpolation points on energy consumption

Interpolation point	Mean value/(kJ·kg^{-1})	Best value/(kJ·kg^{-1})	Worst value/(kJ·kg^{-1})	Standard deviation/(kJ·kg^{-1})
6	34.80	34.46	41.29	43.90
8	33.79	33.51	39.46	41.31
10	36.03	35.18	43.45	46.97
12	1.13	0.84	2.00	2.84

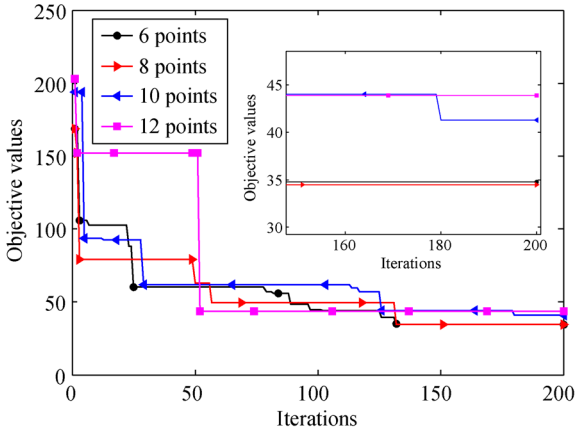

Fig. 8 Convergence histories of the different interpolation points on energy consumption.

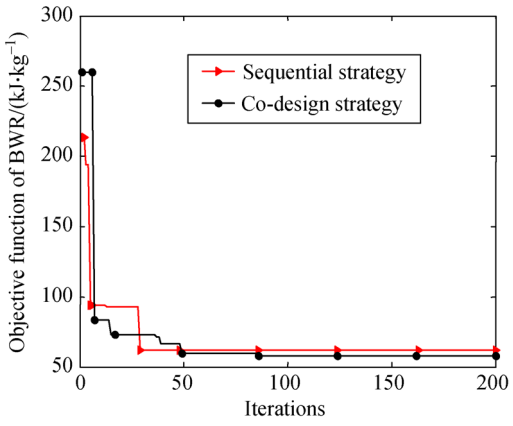

Fig. 9 Convergence histories of co-design strategy and sequential strategy for the bucket wheel reclaimer.

5.2 Optimization of BWR

As mentioned above, eight interpolation points are helpful to achieve the optimal solution and are selected to serve as the control parameters. As shown in Section 3.2, the structural system consists of 27 parameters. In the conventional sequential strategy, the performance of the BWR has been enhanced by optimizing the structural or control parameters. However, these results are sub-optimal solutions because the coupling relationships between the structural and control parameters are ignored. This study adopts the co-design strategy to apply the system optimization problem for addressing the above-mentioned challenge. This strategy can simultaneously optimize multiple sub-disciplines by considering structural and control parameters.

A total of 30 independent runs are performed to obtain the optimal solution for the BWR for minimizing statistical errors. By running the co-design strategy, the optimization results can be obtained, as shown in Fig. 9. Interestingly, the optimal values of sequential strategy are larger than that of co-design strategy. This difference is due to that the sequential strategy ignores the synergy between the subsystems. Specifically, the stable solution can be achieved at the 86th iteration with an optimal value of 57.72 kJ/kg. Table 3 lists the optimized design variables and objective function values. Notably, "+" denotes an increase and "−" denotes a decrease. Evidently, the sequential strategy can obtain the sub-optimal solution, which is 61.86 kJ/kg. Co-design strategy can provide very competitive results than the sequential strategy and initialization values. The results indicate that the optimal solution of co-design strategy is 57.72 kJ/kg, which is 27.31% lower than that of the initial values. From the aforementioned results, we conclude that co-design strategy is credible and can efficiently solve engineering optimization problems.

As discussed in Section 3.1, the control system is an important part of the BWR. The control parameters can be optimized on the basis of the RBF. Figure 10 shows the angular velocity and output power of the motor with the co-design strategy. As shown in Fig. 10(a), the maximum speed of the motor of the rotating system is 0.079 rad/s, which is less than the rated speed of 0.085 rad/s. Furthermore, the speed curve generated by co-design strategy can also meet the requirement of constant volume constraint. The output power of the motor shown in Fig. 10(b) indicates that the maximum output power is close to the extremum with the co-design strategy. This difference is due to that the co-design strategy considers the relationships between subsystems. From the above-mentioned reasons, we conclude that the co-design strategy can effectively improve the motor efficiency and solve real-world optimization problems.

Vibration displacement is used as the dynamic response index to verify the performance of the BWR with different optimization strategies. The sequential strategy is used to compare it with the co-design strategy. Figure 11 shows the vibration displacement of the BWR. Evidently, the vibration displacement of the BWR is periodic in the radial direction. The main reason is that the bucket wheel movement is a circular motion, which causes the periodicity of the cutting resistance. Furthermore, the vibration displacement is relatively stable because of the hierarchical operational strategy. In comparison with the results in Fig. 11, the vibration amplitude of the BWR with co-design strategy is smaller than that with the sequential strategy. This situation is caused by the structural size and stiffness matrix of the BWR. Specifically, the maximum value of co-design strategy is 12.1 mm, which is 5.8 mm smaller than that of the sequential strategy. In this engineering case, the co-design strategy is applied to find the optimal parameters. From the results of different optimization strategies, we conclude that co-design strategy can efficiently solve engineering optimization problems.

Table 3 Optimization results of co-design strategy and sequential strategy for the bucket wheel reclaimer

Design variable	Initial value	Sequential strategy		Co-design strategy	
		Optimal value	Improved/%	Optimal value	Improved/%
x_1	3.50 m	4.19 m	+ 19.71	4.20 m	+ 20.00
x_2	3.50 m	2.64 m	− 24.57	3.53 m	+ 0.83
x_3	3.50 m	2.79 m	− 20.29	2.56 m	− 26.81
x_4	5.60 m	5.33 m	− 4.82	5.50 m	− 1.87
x_5	3.00 m	4.20 m	+ 40.00	4.19 m	+ 39.67
x_6	6.00 m	2.75 m	− 8.33	5.62 m	− 6.26
x_7	3.00 m	2.90 m	− 3.33	3.29 m	+ 9.70
x_8	6.00 m	2.84 m	− 5.33	5.61 m	− 6.53
x_9	3.00 m	2.80 m	− 6.67	2.97 m	− 1.13
x_{10}	6.00 m	2.84 m	− 5.33	5.23 m	− 12.86
x_{11}	1.079×10^{-2} m^2	1.19×10^{-2} m^2	+ 10.28	1.29×10^{-2} m^2	+ 19.49
x_{12}	3.50×10^{-2} m^2	4.46×10^{-2} m^2	+ 27.60	2.77×10^{-2} m^2	− 20.71
x_{13}	2.83×10^{-3} m^2	3.12×10^{-3} m^2	+ 10.35	2.84×10^{-3} m^2	+ 0.37
x_{14}	4.92×10^{-2} m^2	5.07×10^{-2} m^2	+ 3.29	5.25×10^{-2} m^2	+ 6.95
x_{15}	1.08×10^{-2} m^2	1.35×10^{-2} m^2	+ 25.11	1.17×10^{-2} m^2	+ 8.58
x_{16}	7.78 m	8.85 m	+ 13.75	8.89 m	+ 14.25
x_{17}	4.80 m	5.16 m	+ 7.50	4.52 m	− 5.80
x_{18}	1.08×10^{-2} m^2	1.21×10^{-2} m^2	+ 11.95	1.36×10^{-2} m^2	+ 25.87
x_{19}	4.37 m	3.74 m	− 14.42	3.66 m	− 16.25
x_{20}	3.00 m	4.34 m	+ 44.67	2.17 m	− 27.56
x_{21}	4.29×10^{-3} m^2	5.02×10^{-3} m^2	+ 16.94	5.65×10^{-3} m^2	+ 31.71
x_{22}	3.77 m	3.19 m	− 15.38	3.72 m	− 1.22
x_{23}	8.50×10^{-3} m^2	1.12×10^{-3} m^2	+ 31.85	6.98×10^{-3} m^2	− 17.79
x_{24}	70.00°	61.42°	− 12.26	57.79°	− 17.44
x_{25}	9.00°	7.78°	− 13.56	7.78°	− 13.56
x_{26}	26.00°	19.86°	− 23.62	20.96°	− 19.39
x_{27}	9.00°	7.15°	− 20.56	7.20°	− 20.00
v_1	3.00×10^{-2} rad/s	2.72×10^{-2} rad/s	− 9.47	2.61×10^{-2} rad/s	− 13.10
v_2	4.00×10^{-2} rad/s	3.83×10^{-2} rad/s	− 4.24	4.26×10^{-2} rad/s	+ 6.52
v_3	6.50×10^{-2} rad/s	7.96×10^{-2} rad/s	+ 22.51	5.90×10^{-2} rad/s	− 9.29
v_4	8.00×10^{-2} rad/s	7.05×10^{-2} rad/s	− 11.86	7.58×10^{-2} rad/s	− 5.27
v_5	5.80×10^{-2} rad/s	4.92×10^{-2} rad/s	− 15.09	4.88×10^{-2} rad/s	− 15.87
v_6	7.50×10^{-2} rad/s	6.48×10^{-2} rad/s	− 13.58	7.88×10^{-2} rad/s	+ 5.00
v_7	6.30×10^{-2} rad/s	6.19×10^{-2} rad/s	− 1.75	5.07×10^{-2} rad/s	− 19.56
v_8	5.00×10^{-2} rad/s	4.05×10^{-2} rad/s	− 19.04	3.84×10^{-2} rad/s	− 23.24
Best value	79.45 kJ/kg	61.86 kJ/kg	− 22.14	57.72 kJ/kg	− 27.31
Worst value	–	67.59 kJ/kg	− 14.93	63.90 kJ/kg	− 19.57
Mean value	–	64.71 kJ/kg	− 18.55	60.71 kJ/kg	− 23.59
Standard deviation	–	2.14 kJ/kg	1.93	1.95 kJ/kg	1.92

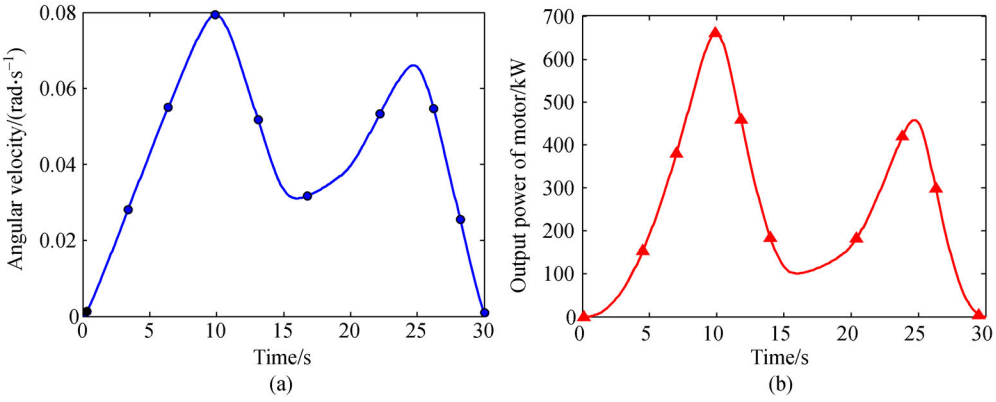

Fig. 10 Speed and power of the motor with co-design strategy: (a) Control speed and (b) output power of the rotation motor.

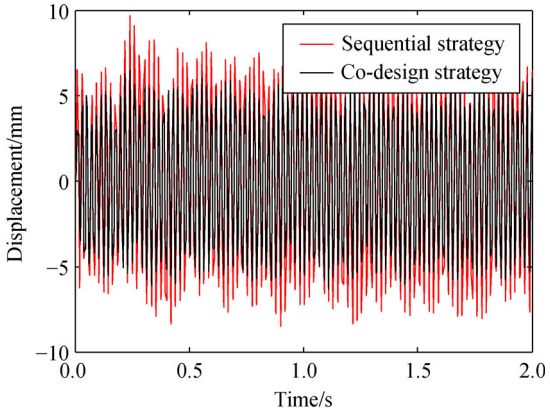

Fig. 11 Dynamic response of the bucket wheel reclaimer with different optimization strategies.

6 Conclusions

This study developed a simultaneous optimal design of structural and control systems for BWR. The conventional optimization strategy usually fails to meet the requirement of optimal results in all disciplines because the BWR includes several disciplines. A co-design strategy was developed to optimize the BWR for addressing this issue by considering structural and control parameters. The BWR was decomposed into some subsystems in accordance with the functions by using the hierarchical decomposition approach. The synergistic relationships between the subsystems were considered using the co-design strategy to minimize the energy consumption per volume. Furthermore, the RBF model was applied for the planning of the rotation speed considering the relationships of subsystems.

The performance of the BWR was evaluated by the co-design and sequential strategies. The results indicate that co-design strategy is more effective than the conventional sequential strategy. The vibration amplitude of the BWR with co-design strategy is smaller than that of the conventional strategy. Thus, the former can be used as an efficient strategy for parameter estimation and prediction of highly nonlinear optimization problems.

However, additional constrains and design parameters and their uncertainties should be considered in future research. For instance, we ignored the uncertainties of parameters and used the maximum installation diameter on the boom, which likely affect the life of the bucket wheel. In the future work, additional subsystems that may cause the vibration will be considered.

Acknowledgements The research was supported by the National Key R&D Program of China (Grant Nos. 2018YFB1700704 and 2018YFB-1702502).

References

1. Bošnjak S M, Arsić M A, Zrnić N Đ, et al. Bucket wheel excavator: Integrity assessment of the bucket wheel boom tie-rod welded joint. Engineering Failure Analysis, 2011, 18(1): 212–222
2. Chatterjee A, Das D. A review of bucket wheel reclaimer failure through mechanical test and metallographic analysis. Journal of Failure Analysis and Prevention, 2014, 14(6): 715–721
3. Bošnjak S, Pantelić M, Zrnić N, et al. Failure analysis and reconstruction design of the slewing platform mantle of the bucket wheel excavator O&K SchRs 630. Engineering Failure Analysis, 2011, 18(2): 658–669
4. Lu T F. Preparation for turning a bucket wheel reclaimer into a robotic arm. In: Proceedings of the International Conference on Robotics and Biomimetics. Bangkok: IEEE, 2008, 1710–1715
5. Lu T F. Bucket wheel reclaimer modeling as a robotic arm. In: Proceedings of the International Conference on Robotics and Biomimetics. Guilin: IEEE, 2009, 263–268
6. Zhao S, Lu T F, Koch B, et al. A simulation study of sensor data fusion using UKF for bucket wheel reclaimer localization. In: Proceedings of the IEEE International Conference on Automation Science and Engineering (CASE). Seoul: IEEE, 2012, 1192–1197
7. Yang L, Qi J, Li S, et al. Collaborative optimization for train scheduling and train stop planning on high-speed railways. Omega,

2016, 64: 57–76

8. Yuan Y L, Song X G, Sun W, et al. Multidisciplinary design optimization of the belt drive system considering both structure and vibration characteristics based on improved genetic algorithm. AIP Advances, 2018, 8(5): 055115
9. Li W, Wang P, Li D, et al. Multiphysical field collaborative optimization of premium induction motor based on GA. IEEE Transactions on Industrial Electronics, 2018, 65(2): 1704–1710
10. Zhao T, Liu D, Chen Q. A collaborative optimization method for heat transfer systems based on the heat current method and entransy dissipation extremum principle. Applied Thermal Engineering, 2019, 146: 635–647
11. Sun W, Wang X B, Wang L T, et al. Multidisciplinary design optimization of tunnel boring machine considering both structure and control parameters under complex geological conditions. Structural and Multidisciplinary Optimization, 2016, 54(4): 1073–1092
12. Sun W, Wang X B, Shi M L, et al. Multidisciplinary design optimization of hard rock tunnel boring machine using collaborative optimization. Advances in Mechanical Engineering, 2018, 10(1): 1687814018754726
13. Huang Z L, Zhou Y S, Jiang C, et al. Reliability-based multidisciplinary design optimization using incremental shifting vector strategy and its application in electronic product design. Acta Mechanica Sinica, 2018, 34(2): 285–302
14. Bidoki M, Mortazavi M, Sabzehparvar M. A new approach in system and tactic design optimization of an autonomous underwater vehicle by using multidisciplinary design optimization. Ocean Engineering, 2018, 147: 517–530
15. Garg D, Patterson M A, Francolin C, et al. Direct trajectory optimization and costate estimation of finite-horizon and infinite-horizon optimal control problems using a Radau pseudospectral method. Computational Optimization and Applications, 2011, 49 (2): 335–358
16. Janson L, Schmerling E, Pavone M. Monte Carlo motion planning for robot trajectory optimization under uncertainty. In: Bicchi A, Burgard W, eds. Robotics Research. Cham: Springer, 2018, 343–361
17. Wang X B, Sun W, Li E Y, et al. Energy-minimum optimization of the intelligent excavating process for large cable shovel through trajectory planning. Structural and Multidisciplinary Optimization, 2018, 58(5): 2219–2237
18. Tian L, Collins C. An effective robot trajectory planning method using a genetic algorithm. Mechatronics, 2004, 14(5): 455–470
19. Franke R. Scattered data interpolation: Tests of some methods. Mathematics of Computation, 1982, 38(157): 181–200
20. Rippa S. An algorithm for selecting a good value for the parameter c in radial basis function interpolation. Advances in Computational Mathematics, 1999, 11(2–3): 193–210
21. Wu Z, Schaback R. Local error estimates for radial basis function interpolation of scattered data. IMA Journal of Numerical Analysis, 1993, 13(1): 13–27
22. He E J. Cantilever wheel arm gyral machine for heaping and taking the material $1/\cos\varphi$ speed control system. The World of Inverters, 2006, 10(5): 106–107 (in Chinese)
23. Chudnovskii V Y. Vertical oscillations of the working unit of a bucket-wheel excavator in a pit face and their suppression. Journal of Machinery Manufacture and Reliability, 2008, 37(3): 221–227
24. Wolpert D H, Macready W G. No free lunch theorems for optimization. IEEE Transactions on Evolutionary Computation, 1997, 1(1): 67–82
25. Yuan Y L, Lv L Y, Wang X B, et al. Optimization of a frame structure using the Coulomb force search strategy-based dragonfly algorithm. Engineering Optimization, 2020, 52(6): 915–931